INTERNATIONAL JOURNAL FOR NUMERICAL AND ANALYTICAL METHODS IN GEOMECHANICS
Int. J. Numer. Anal. Meth. Geomech., **24**, 1–27 (2000)

A RATIONAL METHOD FOR DEVELOPMENT OF LIMIT STATE FOR LIQUEFACTION EVALUATION BASED ON SHEAR WAVE VELOCITY MEASUREMENTS

C. HSEIN JUANG*,† AND CAROLINE J. CHEN‡

Civil Engineering Department, Clemson University, Clemson, SC 29634-0911, U.S.A.

SUMMARY

This papers presents a new approach for developing a limit state for liquefaction evaluation based on field performance data. As an example to illustrate the new approach, a database that consists of, among many other features, *in situ* shear wave velocity measurements and field observations of liquefaction/non-liquefaction in historic earthquakes is analysed. This database is first used to train a neural network to classify liquefaction/non-liquefaction based on soil resistance parameters and load parameters. The successfully trained and tested neural network is then used to establish a limit state, a multiple dimension boundary that separates 'zone' of liquefaction from 'zone' of non-liquefaction. The limit state yields cyclic resistance ratio for a given set of soil resistance parameters. Examination of all cases in the database show that the developed limit state has a high degree of accuracy in predicting the occurrence of liquefaction/non-liquefaction. The developed neural network model can accurately predict the cyclic resistance ratio of soils. Copyright © 2000 John Wiley & Sons, Ltd.

KEY WORDS: liquefaction potential; shear wave velocity; artificial neural network; limit state; simplified chart; case history

INTRODUCTION

Because of the difficulty and the cost in obtaining high-quality undisturbed samples, simplified methods based on *in situ* tests such as the Standard Penetration Test (SPT), the Cone Penetration Test (CPT), the Shear Wave Velocity Test (V_s), and the Becker Penetration Test (BPT) are preferred by geotechnical engineers for evaluating liquefaction potential of soils. In fact, the 'simplified procedure' based on SPT for evaluation of liquefaction potential, developed by the late Professor Seed and his co-workers,[1,2] has become the *standard of practice* in North American and throughout much of the world, although there have been serious criticisms (for example, Reference[3]).

Existing simplified methods such as Seed and Idriss[2] all rely on some 'limit states' that separate liquefaction cases from non-liquefaction cases. These limit states, generally expressed in the form

* Correspondence to: Dr. C. H. Juang, Department of Civil Engineering, Lowry Hall, Box 340911, Clemson University, Clemson, SC 29634-0911, USA. E-mail: hsein@clemson.edu.
† Professor
‡ Research Assistant

Contract/grant sponsor: National Science Foundation, contract grant number: CMS-9612116.

CCC 0363–9061/2000/010001–27$17.50

Received 26 October 1998
Revised 23 February 1999

of empirical charts, are all established based on field observations of soil performance against liquefaction in earthquakes at sites where *in situ* test data are available. Development of a limit state based on historic cases relied heavily on engineering judgment and inevitably induced many uncertainties. Several methods, however, have been proposed to address this issue from a more fundamental point of view. Davis and Berrill[4] have developed energy method for liquefaction assessment. Desai and his associates[5–9] have developed a fundamental model for liquefaction instability analysis based on the Disturbed State Concept (DSC). The DSC 'provides a unified constitutive model for the characterization of entire stress–strain behaviour under cyclic loading, and the values of disturbance at threshold states in the deforming microstructure provides the basis for the identification of liquefaction'. This method, fundamentally, is considered to be an improvement over the simplified methods and the energy-based methods.

In the present study, a new approach based on Artificial Neural Network (ANN) technology is developed, by which limit state can be established *rationally* using historic case records. The V_s-based liquefaction evaluation is used as an example to illustrate this new approach. A large database of case records of liquefaction and non-liquefaction observations collected by Andrus and Stokoe[10] is used for the development of ANN models and the subsequent development of limit state.

The developed V_s-based limit state for liquefaction evaluation is compared with the empirical chart recommended by Andrus and Stokoe.[10] The latter is based on a thorough review of many excellent works on V_s-based liquefaction evaluation[11–16] and subsequent analyses of collected V_s-based liquefaction and non-liquefaction case histories. The proposed new method is shown to be superior to Andrus and Stokoe's.

DEVELOPMENT OF LIMIT STATE

An extensive collection of V_s-based liquefaction and non-liquefaction case histories, documented by Andrus and Stokoe,[10] forms the basis for the development of limit state presented herein. Each case record is interpreted in the present study as

$$\mathrm{LC} = f_1(\sigma'_v, \sigma_v, V_s, \mathrm{ST}, a_{max}, M_w) \tag{1}$$

where LC is the liquefaction class (LC = 1 if liquefaction/marginal liquefaction is observed, LC = 0 if liquefaction is not observed), σ'_v the effective overburden stress, σ_v the total overburden stress, ST the soil type, V_s the shear wave velocity, a_{max} the peak horizontal ground surface acceleration and M_w the earthquake magnitude (moment magnitude).

From data analysis point of view, the problem here is to construct the model f_1 so that for a set of six input variables (σ'_v, σ_v, ST, V_s, a_{max}, M_w), the output (LC) can be correctly predicted. The simplified method based on SPT, developed by Seed and Idriss,[1,2] used a simple mechanism to define a 'limit state', that is, separating liquefaction cases from non-liquefaction cases through visual inspection of data points defined by plotting Cyclic Stress Ratio (CSR) versus *in situ* strength of the soil as measured by the normalized Standard Penetration Resistance $(N_1)_{60}$. This mechanism of separating liquefaction cases from non-liquefaction cases, conceptually illustrated in Figure 1, offers a simple procedure by which the liquefaction potential of a soil can be assessed. This mechanism is also adopted by other simplified methods based on *in situ* tests such as CPT and V_s.[10,17,18]

While existing simplified methods are easy to use and have become the standard of practice in the evaluation of liquefaction potential, there are a couple of main drawbacks. First, considerable

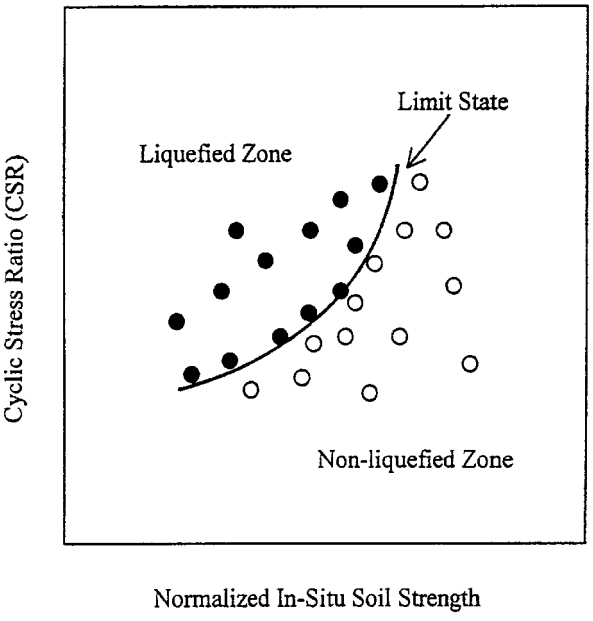

Figure 1. Limit state as a separator for liquefied zone and non-liquefied zone

judgment is required in drawing the limit state curve, which inevitably induces uncertainties into it. The degree of conservatism is hard to quantify, although it is safe to assert that the limit state curve is generally drawn conservatively. Therefore, *consistent* probability measure of liquefaction potential may not be obtained.[19–21] The commonly used Factor of Safety (FS), defined as the ratio of Cyclic Resistance Ratio (CRR), which is the soil resistance based on this limit state, over Cyclic Stress Ratio (CSR) caused by an earthquake, cannot consistently and accurately reflect the degree of safety. Even with the probabilistic approaches, if it is based on this limit state, the accuracy of such probabilistic solution (as in probabilistic seismic hazard analyses) would be compromised. Second, the original limit state curve by Seed and Idriss[1,2] was developed for clean sand and an earthquake magnitude of 7·5. To account for different combinations of factors that affect liquefaction resistance, such as soil types, fines contents, and earthquake magnitudes, different 'discrete' limit state curves were empirically established. Little consideration was given to possible interactions among these soil parameters, and those between resistance and loading, as they were difficult to assess.

Proposed methodology for developing limit state

The 'liquefaction performance' function such as equation (1) is highly non-linear and a more rational approach to defining limit states for liquefaction evaluation is needed. In the present study, neural network approach is taken to construct the model f_1. Neural network technology is a well-established technique for learning structure (model) from examples. Each example is a data pattern that consists of input (in the case of equation (1), there are six variables, including soil resistance parameters and load parameters) and output (in the case of equation (1), the output is

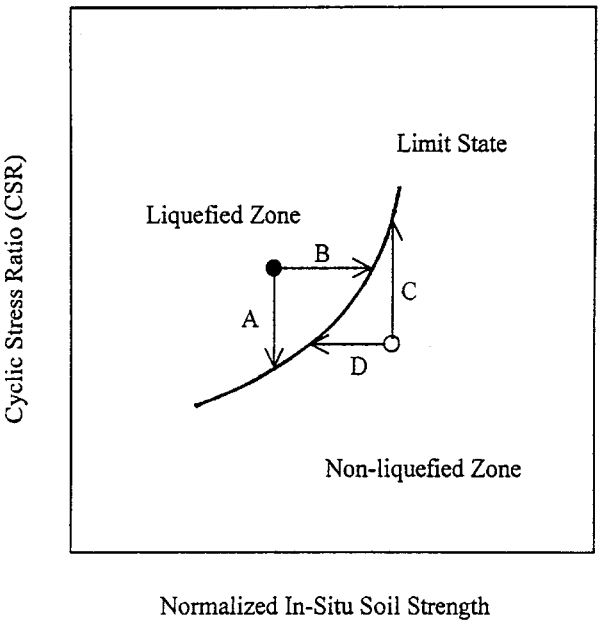

Figure 2. Conceptual model for searching points on limit state

liquefaction observation). Once a neural network is successfully trained and tested to satisfaction, using the collected data (called training patterns and testing patterns, respectively), the model f_1 is constructed.

The model f_1 is a fully connected network with a set of connection weights and biases. This model, a successfully trained network, can easily be implemented in a spreadsheet, and for a given set of input data, the occurrence of liquefaction/non-liquefaction can be predicted. In addition, the limit state can be rationally established using this model. In the present study, the limit state is defined as the 'critical' CSR a soil can resist without liquefaction and beyond which the liquefaction will occur. For a given soil under its *in situ* conditions, this limit state specifies its CRR.

The methodology for establishing the limit state may be illustrated with Figure 2. For each case in the collected database, if liquefaction is observed (output LC = 1), the search for the limit state could involve a reduction of the load parameters a_{max} and M_w (path A in Figure 2) or an increase in normalized soil strength (path B in Figure 2). Considering path A as an example, a new data pattern is formed by decreasing the load parameters a_{max} and M_w while keeping constant the soil resistance parameters (σ'_v, σ_v, ST, and V_s). With new input pattern, the neural network model would produce a new output. Initially, with a small decrease in a_{max} and M_w, the output is likely to remain the same (LC = 1). Continue this process of a_{max} and M_w reduction, however, the output LC will eventually become 0. The average value of a_{max} (and M_w) of the ones before and after the change of LC from 1 to 0 are the load parameters that define the limit state (or the critical CSR). In other words, the CRR for the soil under its *in situ* conditions, as represented by a set of soil resistance parameters (σ'_v, σ_v, ST, and V_s), is equal to the critical CSR that is calculated using the load parameters obtained in the search described above.

If non-liquefaction is observed (the output LC = 0), the search for the limit state could involve an increase in the load parameters a_{max} and M_w (path C in Figure 2) or a decrease in the normalized soil strength (path D in Figure 2). Using path C as an example, a new data pattern is formed by increasing the load parameters a_{max} and M_w while keeping constant the soil resistance parameters (σ'_v, σ_v, ST, and V_s). With new input pattern, the neural network model would produce a new output. Initially, with a small increase in a_{max} and M_w, the output is likely to remain the same (LC = 0). Continue this process to increase a_{max} and M_w, however, the output LC will eventually become 1. The average value of a_{max} (and M_w) of the ones before and after the change of LC from 0 to 1 are the load parameters that define the limit state (or the critical CSR). In other words, the CRR for this soil under its *in situ* conditions, as represented by a set of soil resistance parameters (σ'_v, σ_v, ST, and V_s), is equal to the critical CSR that is calculated using the load parameters obtained in the search described above.

Note that in many cases, the search for the critical CSR may not be successful. Using path C as an example, this may occur when the load parameters have reached the upper bound of typical parameter ranges and yet, the output of the neural network remains unchanged (LC = 0). The reason for that is that some soils are non-liquefiable, as evidenced by the near infinity slope of the upper end of limit state curves in all existing simplified charts (for examples, References 2, 10 and 17). In the cases of paths B and D, the load parameters are kept constant, while the soil resistance parameters are changed until the state of liquefaction/non-liquefaction changes. As in the case of paths A and C, there are situations where the search for the critical CSR by paths B and D may not be successful.

Once critical CSR (or CRR) for all cases that can be determined are obtained, a neural network model may be developed that predicts CRR based on a given set of soil resistance parameters:

$$\mathrm{CRR} = f_2(\sigma'_v, \sigma_v, \mathrm{ST}, V_s) \tag{2}$$

The above procedure creates a CRR model that is independent from the load parameters. In other words, the CRR is a function of soil resistance parameters, not the load parameters. The developed CRR model represents a 'true' limit state (at least to the extent that is supported by the collected case histories). This is a significant improvement over the existing empirical charts that separate liquefaction cases from non-liquefaction cases. Further detail on the development of this new limit state based on V_s measurement is presented in the sections that follow.

Prediction of the occurrence of liquefaction—neural network approach

As described in the above section, the first step in the development of V_s-based limit state for calculating CRR is to train neural network with the collected V_s-based case histories. The process begins with selection of input variables or parameters. In the present study, it is determined that use of six input variables (σ'_v, σ_v, V_s, ST, a_{max}, M_w) yields the best results. The ANN model adopted for all subsequent analyses is

$$\mathrm{LCI} = f_3(\sigma'_v, \sigma_v/\sigma'_v, V_s/\sigma'_v, \mathrm{SCN}, a_{max}, M_w) \tag{3}$$

This ANN model essentially follows the conceptual model represented by equation (1) with a few modifications. First, the output variable is changed from Liquefaction Class (LC) to Liquefaction Class Indicator (LCI) to reflect the fact that while the target is either 0 (non-liquefaction) or

Table I. Soil class numbers

Soil description	Soil class number (SCN)
Gravel and gravelly sand with less than 5–10% fines	4
Clean sand with less than 5% fines	3
Sand mixture to sand (fines content between 5 and 15%)	2·5
Sand mixtures: sandy silt to silty sand (fines content between 15 and 35%)	2
Silt to sand mixtures (fines content between 35 and 70%)	1·5
Silt mixtures: silty clay to clayey silt	1

1 (liquefaction) in a data pattern, the actual output from the neural network is a real value between 0 and 1. Following the conventional interpretation of neural network output, a case is classified as 'liquefied' (and thus, LC = 1) if LCI > 0·5, and it is classified as 'non-liquefied' (LC = 0) if LCI < 0·5. Second, to closely follow the common geotechnical engineering practice in normalizing the *in situ* strength parameter with respect to the effective overburden stress, the ratios of σ_v/σ'_v and V_s/σ'_v are used in lieu of σ_v and V_s, respectively. Different stress exponent, the parameter n in the expression of $V_s/(\sigma'_v)^n$, has been suggested for normalization (for example, Liao *et al.*[20] used $n = 0{\cdot}5$ for SPT; Robertson *et al.*[13] used $n = 0{\cdot}25$ for V_s). Olsen[22] argued that the stress exponent for normalization should be a variable depending on soil type and *in situ* stress conditions. From dimensional consistency point of view, a dimensionless argument, namely $[V_s(g\,\sigma'_v/\gamma)^{0{\cdot}5}]$, where g is the acceleration of gravity and γ is the unit weight of soil, could be a better one to use in the ANN model. In the present study, however, only the simplest form of normalization (V_s/σ'_v) is used, as the issue of stress exponent would be implicitly addressed by the highly-nonlinear nature of network connections.

The variable ST (for soil type) in equations (1) and (2) is now more specifically called Soil Class Number (SCN) for subsequent neural network development. The range of SCN is shown in Table I, which is consistent with soil descriptions given in the database compiled by Andrus and Stokoe.[10] According to Andrus (personal communication, 1998), soil-type description given in the database is based primarily on particle size information. The four *basic* soil types are gravel, sand, sand mixture, and silt mixture, each of them assigned an SCN ranging from 1 to 4. Intermediate class with SCN = 1·5 or 2·5 is allowed in the present study, using fines content as a guide. While the variable SCN is only a category index, the neural network yields much better prediction with it.

Training neural networks for predicting liquefaction potential based on published case histories is, of course, nothing new.[23–27] However, this is just one step in the proposed methodology for development of a limit state. The development of neural network based on the model f_3 (equation (3)) is presented below.

Data source and data preprocessing: The database of V_s-based liquefaction and non-liquefaction case histories, compiled by Andrus and Stokoe,[10] forms the basis of the present study. A few cases at Larter Ranch and Whiskey Springs were excluded from consideration by Andrus and Stokoe,[10] as 'the soils at these two sites may be weakly cemented with carbonate'. These cases are not considered in the present study. Thus, a total of 186 data patterns are available for the present study. One hundred and thirty (130) cases, about 70 per cent of all cases, are selected for

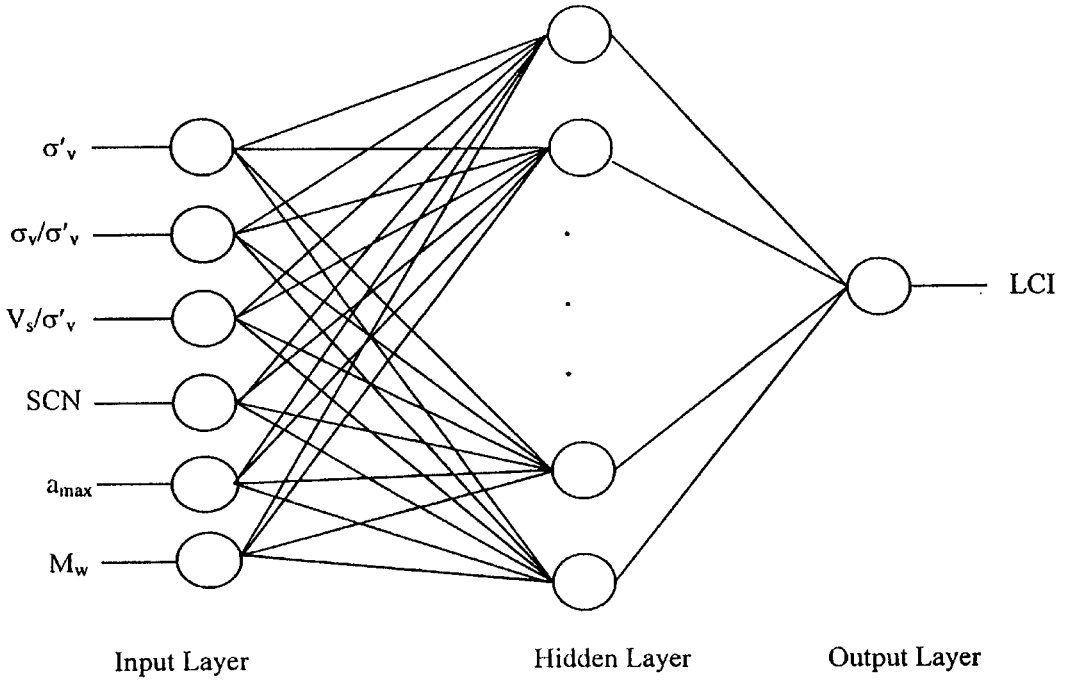

Figure 3. Elements of a three-layer artificial neural network

training the neural network, and the rest (56 cases) are used for testing the trained network. Note that in the original database, cases labeled as 'marginal liquefaction' are treated as 'liquefaction' cases. In other words, the target (desired output of the data patterns) is either LCI = 0 or 1.

Scaling of input parameters is generally required as the preprocessing step of the network training. In the present study, all input parameters are scaled with respect to the minimum and the maximum into the range of 0·1–0·9. Symbolically, this scaling procedure is expressed:

$$x_{\text{norm}} = (x + a)/b \tag{4}$$

where

$$a = (x_{\max} - 9x_{\min})/8 \tag{4a}$$

$$b = (x_{\max} - x_{\min})/0{\cdot}8 \tag{4b}$$

and where x is the actual parameter value, $x_{\min}$ and $x_{\max}$ are the minimum and maximum value, respectively. The output parameter or target is left as 0 or 1.

Neural network topology, training algorithm and implementation: A three-layer, feed-forward network topology, as shown in Figure 3, is adopted in this study for its simplicity and effectiveness. The number of neurons in the hidden layer is determined through a trial-and-error

process, as is normally done in back-propagation neural networks. Seven hidden neurons are selected, since it is the smallest number of neurons that are required to yield satisfactory results (judged by the network performance) in the present study. The transfer functions adopted in the present study are 'sigmoid' function defined below:

$$f_4(\theta) = 1/(1 + e^{-\theta}) \tag{5}$$

The training algorithm generally adopted is either the backpropagation technique with a learning rate and a momentum term or the Levenberg-Marquardt (LM) algorithm.[28] The LM algorithm, defined below, is adopted in this study for its efficiency in training networks:

$$\Delta W = (J^{\mathrm{T}}J + \lambda I)^{-1}J^{\mathrm{T}}e \tag{6}$$

where J is the Jacobian matrix of derivatives of each error with respect to each weight, I is an identity matrix, λ is a scalar, and e is an error vector. If a very large λ value is used, the LM algorithm is approximately the same as the gradient descent method, as $J^{\mathrm{T}}J$ term becomes negligible and the weight change is controlled by $\lambda^{-1}J^{\mathrm{T}}e$, which is the gradient descent. If the λ value is very small, this equation becomes the Gauss–Newton method, which is much faster in locating the minimum error. In the present study, the LM algorithm implemented in a toolbox of MATLAB,[29] called neural network toolbox,[28] is used for training network. The neural network is trained until it meets the error 'goal' of 0·005, where the network error ('mean squared error') is defined as

$$E = \frac{1}{p}\sum_{j=1}^{p}(z_j - o_j)^2 \tag{7}$$

where p is the number of data patterns used in the training, z_j is the network prediction (i.e. actual network output), and o_j is the target output. This formulation is valid for networks with a single output neuron, as is the case in the present study.

MATLAB provides an interactive computing environment with hundreds of built-in functions, as well as a 'C-like' programming language. Its neural network toolbox contains source codes of various training algorithms that can easily be modified to adapt to different situations. MATLAB is also tied with spreadsheet software such as Excel through a macro called ExcelLink that allows MATLAB commands to be issued from within Excel. This feature greatly eases the data manipulation and sharing between programs.

Results and discussions: Figure 4 shows the reduction of network error in the training process. For this particular problem, the error goal was met after 37 epochs (note: one complete presentation of the entire set of training patterns to the network is an epoch). Figure 5 shows the predicted LCI values for all cases. Taking the conventional interpretation of neural network results (for the problem at hand, it means that liquefaction is said to occur if LCI $>$ 0·5, and no liquefaction occurs if LCI $<$ 0·5), there is only one misclassification. The success rate for correct predictions of the occurrence of liquefaction or non-liquefaction is 100 per cent using the 130 training patterns, and the success rate is about 98 per cent during network testing (one miss in 56 tests). The results from the testing phase show that the trained network is able to 'generalize' the input/output relationship. Being able to generalize this relationship from the training data

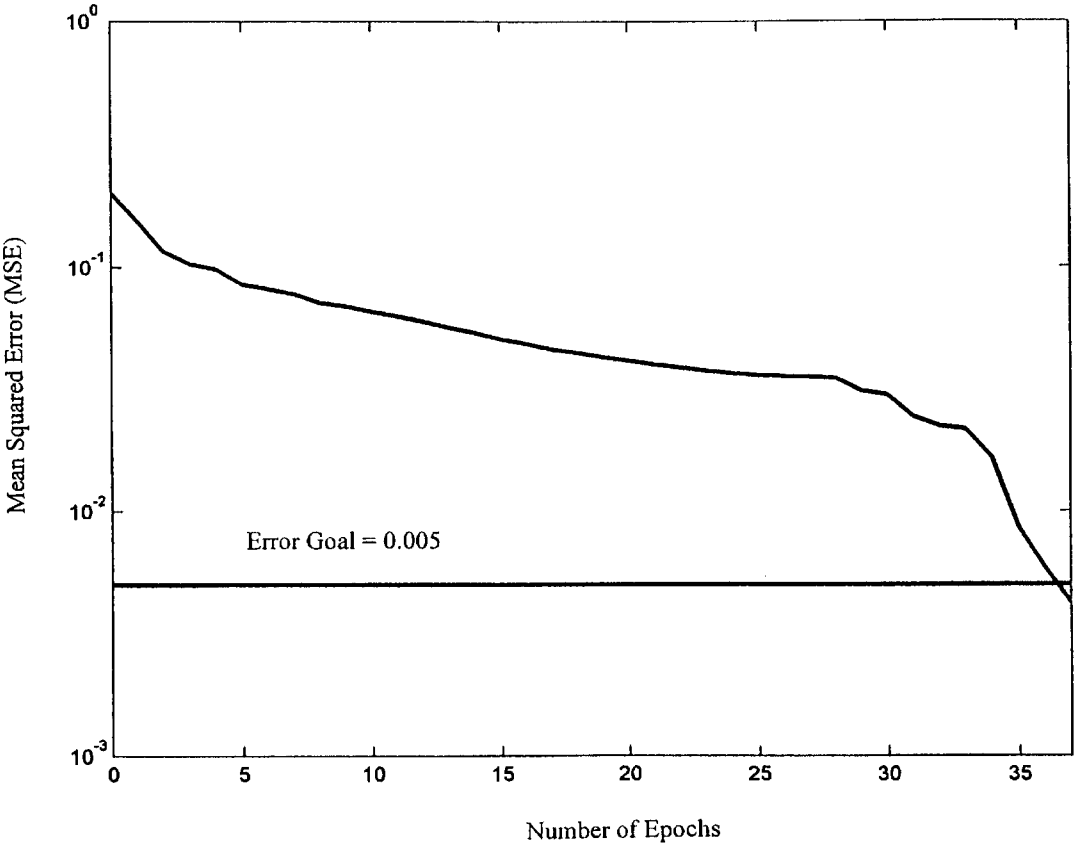

Figure 4. Training a neural network—reduction of network error

patterns is perhaps the single most important feature of neural network technology. The developed network is shown to be able to predict with very high accuracy whether liquefaction will occur or not for a given soil in a given *in situ* condition under a given seismic load.

Comparison with Andrus and Stokoe's chart: Andrus and Stokoe[10] recommended the following equation for determining CRR of uncemented, Holocene-age soils based on V_s-measurements:

$$\mathrm{CRR} = 0{\cdot}03\ (V_s/100)^2 + 0{\cdot}9\ [1/(V_{slc} - V_{sl}) - 1/V_{slc}] \tag{8}$$

where

$$V_{sl} = V_s\ (100/\sigma'_v)^{0{\cdot}25} \tag{8a}$$

V_s is the measured shear wave velocity (m/s) and V_{slc} is a constant with the following values: 220 for sands and gravels with FC $\leqslant$ 5 per cent, 210 for sands and gravels with FC $\approx$ 20 per cent, 200 for sands and gravels with FC $\geqslant$ 35 per cent.

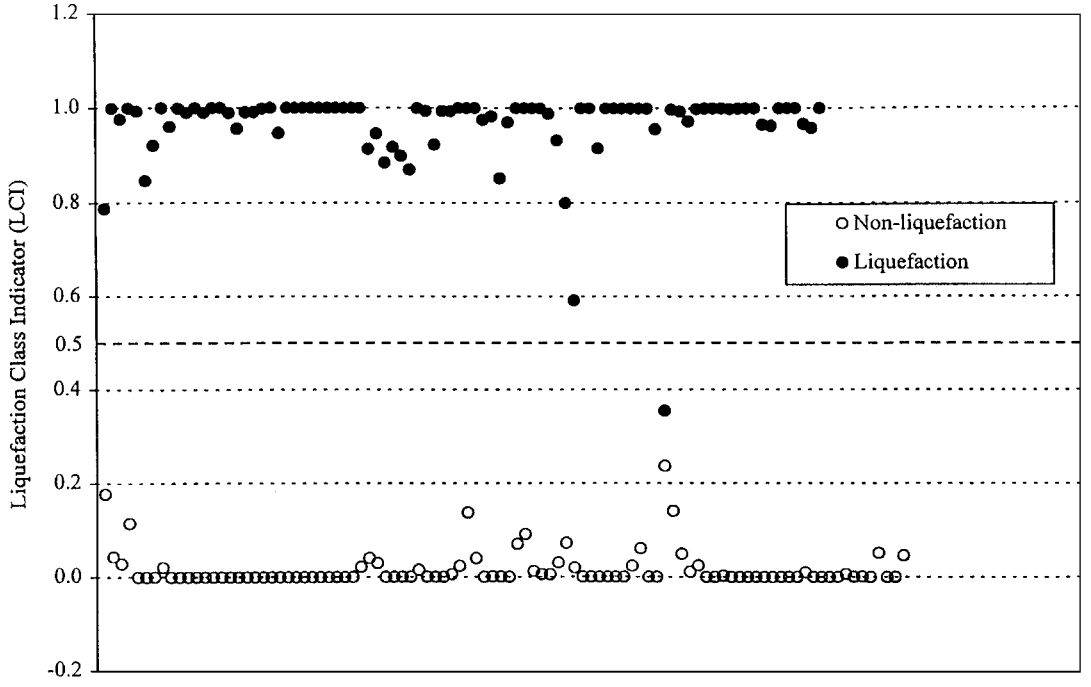

Figure 5. Distribution of liquefaction class indicator (LCI) values for all cases

The equivalent CSR value may be calculated with the following equation:

$$\mathrm{CSR} = 0{\cdot}65\left(\frac{\sigma_v}{\sigma_v'}\right)\left(\frac{a_{max}}{g}\right)(r_d)/\mathrm{MSF} \tag{9}$$

where σ_v', σ_v and a_{max} are same as defined in equation (1), g the acceleration of gravity, r_d the stress reduction coefficient, and MSF the magnitude scaling factor.

The stress reduction factor r_d provides an approximate correction for flexibility of the soil profile. For a depth z of less than 80 ft, the term r_d may be calculated using the following equation:[30]

$$\ln(r_d) = \alpha(z) + \beta(z)M_w \tag{10}$$

where

$$\alpha(z) = -1{\cdot}012 - 1{\cdot}126\sin[(z/38{\cdot}5) + 5{\cdot}133] \tag{10a}$$

$$\beta(z) = 0{\cdot}106 + 0{\cdot}118\sin[(z/37{\cdot}0) + 5{\cdot}142] \tag{10b}$$

The term MSF may be calculated using the following equation:[30]

$$\mathrm{MSF} = 37{\cdot}9\,(M_w)^{-1{\cdot}81} \tag{11}$$

According to Idriss,[30] MSF should be limited to 1·625 for $M_w \leqslant 5{\cdot}75$. Thus, CSR may be calculated by combining equations (9)–(11).

Using the above equations to calculate CRR and CSR, each of the case histories in the database can be evaluated for the occurrence of liquefaction. The results show that the Andrus and Stokoe's method has a success rate of 99 per cent in predicting liquefied cases, a success rate of 40 per cent in predicting non-liquefied cases, and an overall success rate of 68 per cent. Here, 'success' is defined as being able to correctly predict whether liquefaction occurs or not. In other words, the prediction is considered a success if calculated CRR $>$ CSR and no liquefaction is observed. It is also considered a success if calculated CRR $<$ CSR and liquefaction is observed. The Andrus and Stokoe's method appears to have been *conservatively* formulated so that it can have a much greater success rate in predicting liquefied cases. However, any method can have a 100 per cent success rate in predicting only liquefied cases if the CRR is 'artificially' lowered to the extreme. The success rate of 40 per cent in predicting non-liquefied cases and an overall success rate of 68 per cent from the Andrus and Stokoe's method suggests that it is far from being perfect in defining a limit state. On the other hand, the developed neural network (model f_3), with a success rate of greater than 99 per cent in all cases, is seen to be more accurate than the Andrus and Stokoe's method in predicting the occurrence of liquefaction/non-liquefaction. This neural network, however, does not prescribe limit state explicitly, hence additional work is needed.

Development of limit state

The methodology for developing a limit state has been described earlier. The limit state is defined herein as some multiple-dimension 'boundary' that separates liquefaction zone from non-liquefaction zone. Existing simplified charts are all established based on the premise that zones of liquefaction and non-liquefaction can be separated by a simple relation between the critical CSR and some normalized *in situ* soil strength index (such as $(N_1)_{60}$, V_{s1}, or normalized cone tip resistance q_{c1}). Although guided by actual case records, the limit state in the existing simplified charts is subjectively drawn with unknown degree of conservatism. Thus, it would be desirable to be able to rationally construct the limit state. In this regard, the energy method proposed by Davis and Berrill[4] and the disturbed state concept and theory proposed by Desai *et al.*[9] are very significant advancement. In the present study, a different approach to the development of a V_s-based limit state based on the trained ANN model is taken. This approach is described below.

Following paths A and C as described earlier, the critical CSR for each case history may be determined by changing the values of the two load parameters, a_{max} and M_w. Because a_{max} is related to M_w and the distance from the epicentre (R), the iterative process to find the 'right' load parameters (called critical load parameters herein) can focus on one of them. For example, if the term M_w is used in the iteration, then in the iterative process, a_{max} can be changed according to the change made to M_w. In the iterative process, the critical load parameters are found when there is a change of liquefaction prediction (from yes to no or vice versa). In the present study, the following attenuation relation is adopted:[31]

$$a_{max} = 0{\cdot}0185\, e^{1{\cdot}28M}[R + 0{\cdot}147\, e^{-0{\cdot}732M}]^{-1{\cdot}75} \tag{12}$$

where R is the distance to the epicentre and M the earthquake magnitude.

The magnitude M is defined as surface-wave magnitude (M_s) when both local magnitude (M_L) and surface-wave magnitude are greater than 6·0, and it is defined as local magnitude when both

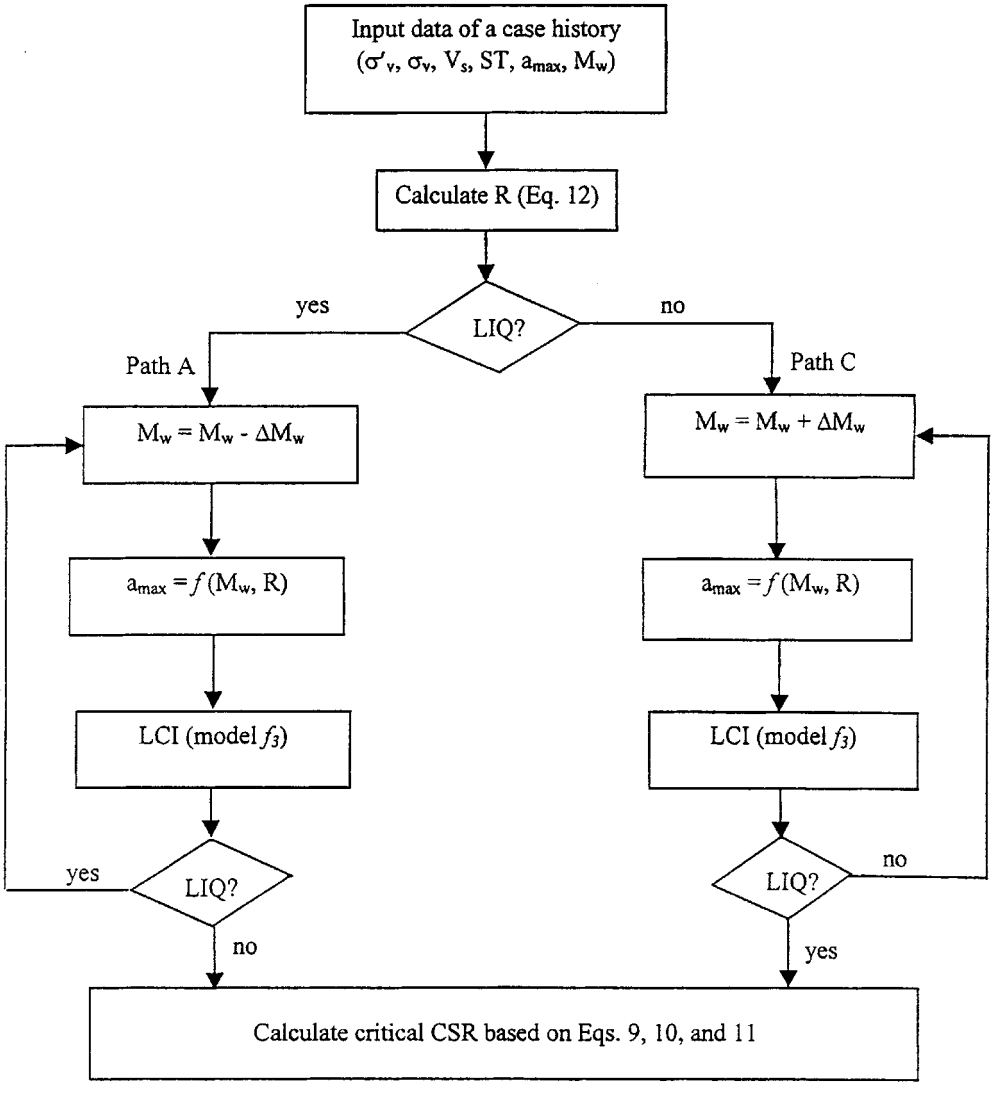

Figure 6. Processes of searching for critical Cyclic Stress Ratio (CSR)

magnitudes are below this value. When the magnitude is between 5 and 8, the difference between M_w and M is insignificant.

For each case history, the term R was back calculated using the above equation with given a_{max} and M. The relation defined in this equation was then used to 'regulate' the change in a_{max} for a given change in M_w in the iterative process. Once the critical load parameters were found, they were used to calculate the critical CSR (and thus CRR) using equations (9)–(11). Figure 6 shows a flowchart of this process in search of the critical CSR using the developed ANN model. This process was repeated for all cases. Note that in many cases, the process could not produce

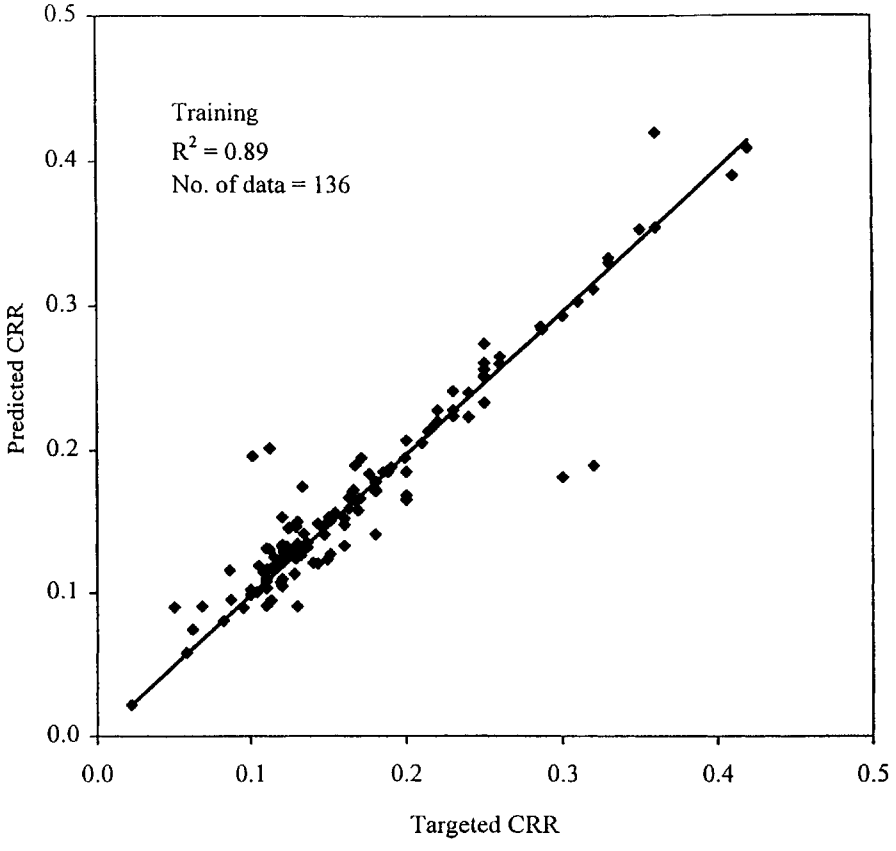

Figure 7. Neural network approximation of Cyclic Resistance Ratio (CRR)—training data

a change in liquefaction class from one to the other without a drastic change in the load parameters, as some soils simply cannot be liquefied or very hard to liquefy. If the load parameters went beyond normal ranges, the corresponding case was excluded from further consideration. In addition, there were situations where more than one case with the same soil (resistance) parameters yielded the same CSR through this search process. In such cases, only one data pattern (critical CSR versus a set of soil parameters, σ'_v, σ_v/σ'_v, V_s/σ'_v, and SCN) was recorded. Following these simple rules, 95 data patterns were obtained.

As described earlier, limit state may also be reached by changing the resistance parameters (paths B and D). With this approach, the load parameters are kept constant, while the resistance parameters are varied until a change in liquefaction class from one to the other occurs. While there might exist several possible combinations of the changes that would result in a change in liquefaction class, it was decided to change only the term V_s/σ'_v, as it provides a simple mechanism that can easily be incorporated in the search process for critical CSR. Using this approach (path B or D) and applying similar rules as adopted in paths A and C, 86 data patterns were obtained.

Thus, a total of 181 limit-state data patterns were obtained. These data patterns were then used to train a neural network based on the conceptual model defined in equation (2). The trained

neural network is essentially an approximation of the 'true' but unknown functional relationship between the input (soil resistance parameters) and the output (CRR). Using a three-layer, feed-forward network topology, a set of connection weights and biases can be obtained through training, which can then be used to 'predict' CRR:[25–26]

$$\mathrm{CRR} = f_6\left\{B_O + \sum_{k=1}^{n}\left[W_k \cdot f_5\left(B_{Hk} + \sum_{i=1}^{m} W_{ik} P_i\right)\right]\right\} \tag{13}$$

where B_O is the bias at the output layer (just one neuron in this layer), W_k the weight of connection between neuron k of the hidden layer and the single output layer neuron, B_{Hk} the bias at neuron k of the hidden layer ($k = 1, n$), W_{ik} the weight of connection between input variable i ($i = 1, m$) and neuron k of the hidden layer, P_i the input parameter i, $f_5(\theta)$ the transfer function of each neuron in the hidden layer and $f_6(\theta)$ the transfer function of the neuron in the output layer.

In the above equation, the number of input variables (m) is 4 and the number of hidden neuron (n) is 12. The input variables are: $P_1 = \sigma_v/\sigma'_v$, $P_2 = \sigma'_v$, $P_3 = \mathrm{SCN}$, and $P_4 = V_s/\sigma'_v$. Note that all input and output variables are normalized into values in the range of 0·1–0·9 using equation (4). Both transfer functions $f_5(\theta)$ and $f_6(\theta)$ adopted in the present study are a 'sigmoid' function, same as the one defined in equation (5). The issues of data preprocessing, training algorithm and implementation in a feed-forward network have been discussed earlier and not to be repeated here. The connection weights and biases obtained for this network are shown in Table II. These weights and biases along with equation (13) define the 'limit state'.

Perhaps, the most efficient way to show the accuracy of the neural network approximation is to plot the 'predicted' CRR versus the 'target (or known)' CRR. Figures 7 and 8 show such a plot for the developed network in training and testing phases, respectively. The neural network model (equation (13) and Table II) to calculate CRR, and equations (9)–(11) to calculate CSR, all cases in the Andrus and Stokoe's database can be assessed, and the results are shown in Table III. A sample calculation is given in the Appendix showing how the developed neural network (equation (13)) is used to determine CRR.

The newly developed neural network-based method has a success rate of 88 per cent in predicting either liquefied or non-liquefied cases, and thus, the overall success rate is also 88 per cent (see Table IV). This represents a significant improvement over the Andrus and Stokoe's method that has an overall success rate of 68 per cent. As discussed earlier, the Andrus and Stokoe's method appears to have been *conservatively* formulated so that it can predict liquefied cases with greater success rate (but at the expense of the success rate for non-liquefied cases). If the developed ANN-based model is applied with a reduction factor of 0·8 for conservative reasons, the success rates for correctly predicting liquefied cases increases to 99 per cent, while the success rate for non-liquefied cases reduces to 70 per cent and the overall success rate becomes 87 per cent. However, to construct a limit state, a 'good' method should be able to correctly predict both liquefied cases and non-liquefied cases. The issue of conservatism should be separated from that of the construction of limit state. The former could be dealt with by selecting an appropriate factor of safety in a deterministic approach or an acceptable level of risk in a probabilistic approach.

Note that the success rate defined earlier and used in the above discussions *could* be somewhat misleading. The potential error in the determination of CSR may exceed the difference between CSR and CRR and thus compromises a meaningful assessment of whether a prediction is correct. This issue is best handled by conducting probabilistic analyses such as Juang *et al.*[21] An

Table II. Connection weights and bias of neural network defined in equation (13)

	Weight					Bias	
	W_{ik}				W_k	B_k	B_0
	Input 1 ($i = 1$)	Input 2 ($i = 2$)	Input 3 ($i = 3$)	Input 4 ($i = 4$)	Output neuron	Hidden layer	Output layer
Hidden neuron 1 ($k = 1$)	−10·372	16·714	− 21·652	0·747	47·461	12·424	55.6464
Hidden neuron 2 ($k = 2$)	77·963	− 46·036	99·919	− 55·755	− 80·242	− 86·903	
Hidden neuron 3 ($k = 3$)	47·182	− 25·345	− 29·461	− 24·476	1·418	10·885	
Hidden neuron 4 ($k = 4$)	189·793	7·139	− 258·829	− 85·802	−1·198	4·619	
Hidden neuron 5 ($k = 5$)	184·536	101·517	135·412	111·656	78·050	− 274·335	
Hidden neuron 6 ($k = 6$)	2·693	1·204	65·308	− 0·850	− 56·401	− 29·746	
Hidden neuron 7 ($k = 7$)	− 8·999	14·155	−18·817	0·454	− 52·780	11·011	
Hidden neuron 8 ($k = 8$)	59·474	− 58·158	− 286·057	− 95·720	− 55·098	147·803	
Hidden neuron 9 ($k = 9$)	− 4·823	17·137	5·219	1·749	3·927	−10·915	
Hidden neuron 10 ($k = 10$)	− 55·142	77·528	−157·690	− 41·533	− 78·274	136·816	
Hidden neuron 11 ($k = 11$)	0·530	16·887	− 52·199	15·045	81·232	28·846	
Hidden neuron 12 ($k = 12$)	− 26·751	77·475	62·682	− 98·634	−1·788	− 61·560	

alternative is to examine this problem with different definitions of success rate. In the subsequent analysis, the definition of 'success is extended to the cases where the method does not yield correct prediction but the difference between the calculated CRR and CSR is less than, say, 5 per cent (or 10 per cent, or even 20 per cent). With this revised definition, the success rates for the newly developed ANN-based model and the Andrus and Stokoe's method are recalculated, and the results are also shown in Table IV. The results show that the developed neural network yields a better limit state for predicting liquefaction resistance CRR.

SUMMARY AND CONCLUSIONS

In the present study, a new method for predicting CRR based on V_s measurement has been developed. Detail in the development of the new method has been presented. The new method is established through three stages: (1) development of an ANN model that predicts liquefaction class for a given set of resistance and load parameters, (2) search for data patterns that collectively define the limit state based on ANN model, and (3) development of another ANN model that

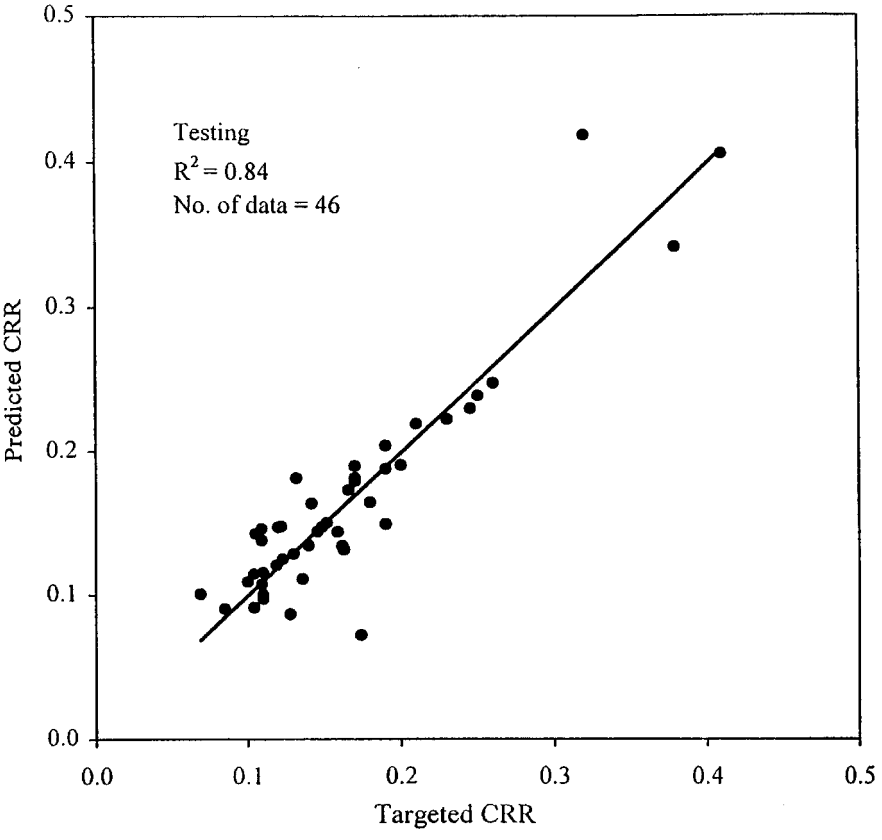

Figure 8. Neural network approximation of Cyclic Resistance Ratio (CRR)—testing data

predicts CRR. The developed method yields accurate predictions of CRR based on V_s. However, more data covering wider ranges of soil and load parameters are needed to further validate the developed method. In addition, in order to address the issue of the uncertainty associated with the data and the CRR model and the issue of the selection of factor of safety for design purpose, probabilistic analyses such as Juang *et al.*[21] could be performed. This is the subject of an on-going research at Clemson University.

Two limitations of using V_s to evaluate liquefaction resistance, according to Andrus and Stokoe,[10] are: (1) field seismic measurements are made with small strains, whereas liquefaction is a large-strain phenomenon, and (2) seismic testing does not provide samples for classification of soils. These limitations should be recognized when attempting to use any V_s-based method for evaluating liquefaction resistance. The conclusions drawn from the present study include:

1. The ANN model developed for predicting liquefaction occurrence, model f_3, can separate liquefaction cases from non-liquefaction cases. The success rate is 100 per cent in the training phase and 98 per cent in the testing phase. This neural network model represents a significant tool that may be used to investigate liquefaction potential of soils under various

Table III. Prediction liquefaction resistance—proposed method versus Andrus—Stokoe's method (source data from Andrus and Stokoe[10])

Site	Depth (m)	σ_v (kPa)	σ'_v (kPa)	Soil type	Average V_s (m/s)	Average a_{max} (g)	Mw	CSR	CRR (ANN)	CRR (Andrus)	Liquefaction observation
(a) *1906 San Francisco, California earthquake* ($M_w = 7{\cdot}7$)											
Coyote Creek	4·75	83·6	62·1	4	136	0·36	7·7	0·32	0·07	0·08	Yes
	4·75	75·4	58·2	4	154	0·36	7·7	0·31	0·15	0·11	Yes
	4·75	75·4	58·2	4	161	0·36	7·7	0·31	0·16	0·12	Yes
	4·75	75·4	58·2	4	173	0·36	7·7	0·31	0·17	0·15	Yes
Salinas River, North	9·85	178·2	140·8	1·5	177	0·32	7·7	0·25	0·25	0·10	No
	9·85	178·2	140·8	1·5	195	0·32	7·7	0·25	0·27	0·13	No
	9·85	178·2	140·8	1·5	200	0·32	7·7	0·25	0·28	0·15	No
	9·85	178·2	140·8	1·5	199	0·32	7·7	0·25	0·27	0·15	No
Salinas River, South	8·75	142·2	123·5	2·5	131	0·32	7·7	0·24	0·21	0·05	Yes
	8·75	142·2	123·5	2·5	149	0·32	7·7	0·24	0·22	0·07	Yes
	8·75	142·2	123·5	2·5	158	0·32	7·7	0·24	0·22	0·08	Yes
	8·75	142·2	123·5	2·5	168	0·32	7·7	0·24	0·22	0·09	Yes
(b) *1964 Niigata, Jaopan earthquake* ($M_w = 7{\cdot}5$)											
Niigata City	6·25	110·9	97·7	3	163	0·16	7·5	0·11	0·15	0·09	No
	4·85	90	54·7	3	115	0·16	7·5	0·17	0·09	0·06	Yes
	3·6	67·8	44·5	3	118	0·16	7·5	0·16	0·08	0·07	Yes
(c) *1975 Haicheng, PRC earthquake* ($M_w = 7{\cdot}1$)											
Paper Mill	4	54·7	35·3	1	122	0·12	7·1	0·11	0·09	0·09	Yes
Glass Fiber	4·75	90	50·1	1·5	98	0·12	7·1	0·12	0·10	0·05	Yes
Construction Building	7·25	124·9	73·7	1	103	0·12	7·1	0·11	0·09	0·04	Yes
Fishery & Shipbuilding	4·5	81·7	43·6	1	101	0·12	7·1	0·13	0·09	0·05	Yes
Middle School	10·25	191·8	101·2	1	143	0·12	7·1	0·12	0·11	0·07	No
Chemical Fiber	8·75	159·4	90·1	1·5	147	0·12	7·1	0·11	0·11	0·08	Marginal
(d) *1979 Imperial Valley, California earthquake* ($M_w = 6{\cdot}5$)											
Wildlife	4·65	83·8	53·9	1·5	127	0·13	6·5	0·10	0·18	0·08	No
	4·65	83·8	53·9	1·5	124	0·13	6·5	0·10	0·18	0·07	No
	4·65	91·8	57·8	1·5	115	0·13	6·5	0·10	0·16	0·06	No
Radio Tower	4·4	79·2	55·8	2	90	0·21	6·5	0·14	0·13	0·04	Yes
McKim	3·15	54·3	38·1	2	126	0·51	6·5	0·36	0·19	0·09	Yes
Vail Canal	4·1	70·4	54·8	2·5	101	0·12	6·5	0·07	0·12	0·05	No
Kornbloom	4·25	74·7	57·8	1	105	0·12	6·5	0·07	0·12	0·05	No

Table III. Continued

Site	Depth (m)	σ_v (kPa)	σ'_v (kPa)	Soil type	Average V_s (m/s)	Average a_{max} (g)	Mw	CSR	CRR (ANN)	CRR (Andrus)	Liquefaction observation
Heber Road, channel fill	3·65	63	48	2	131	0·5	6·5	0·32	0·09	0·09	Yes
	3·65	63	48	2	133	0·5	6·5	0·32	0·13	0·09	Yes
Heber Road, point bar	3·15	60·1	46·6	2·5	164	0·5	6·5	0·32	0·20	0·19	No
	3·15	60·1	46·6	2·5	173	0·5	6·5	0·32	0·20	1·60	No
(e) *1980 Mid-Chiba, Japan earthquake* ($M_w = 5·9$)											
Owi Island, No. 1	6·15	105·4	59·2	2	155	0·08	5·9	0·05	0·15	0·12	No
	14·8	251·6	120·2	2	195	0·08	5·9	0·05	0·42	0·16	No
(f) *1981 Westmorland, California earthquake* ($M_w = 5·9$)											
Wildlife	4·65	83·8	53·9	1·5	127	0·27	5·9	0·17	0·18	0·08	Yes
	4·65	83·8	53·9	1·5	124	0·27	5·9	0·17	0·18	0·07	Yes
	4·65	91·8	57·8	1·5	115	0·27	5·9	0·17	0·16	0·06	Yes
Radio Tower	4·4	79·2	55·8	2	90	0·2	5·9	0·11	0·13	0·04	Yes
McKim	3·15	54·3	38·1	2	126	0·06	5·9	0·03	0·19	0·09	No
Vail Canal	4·1	70·4	54·8	2·5	101	0·3	5·9	0·15	0·12	0·05	Yes
Kornbloom	4·25	74·7	57·8	1	105	0·36	5·9	0·18	0·12	0·05	Yes
Heber Road, channel fill	3·65	63	48	2	131	0·02	5·9	0·01	0·09	0·09	No
	3·65	63	48	2	133	0·02	5·9	0·01	0·13	0·09	No
Heber Road, point bar	3·15	60·1	46·6	2·5	164	0·02	5·9	0·01	0·20	0·19	No
	3·15	60·1	46·6	2·5	173	0·02	5·9	0·01	0·20	1·60	No
(g) *1983 Borah Peak, Idaho earthquake* ($M_w = 6·9$)											
Pence Ranch	2·75	57·2	46·2	4	107	0·36	6·9	0·25	0·13	0·06	Yes
	2·9	52·7	40·5	4	94	0·36	6·9	0·26	0·13	0·05	Yes
	2·3	44·5	36	4	102	0·36	6·9	0·25	0·14	0·06	Yes
	3·2	62·1	49·4	4	109	0·36	6·9	0·25	0·13	0·06	Yes
	2·45	60·5	45·6	4	122	0·36	6·9	0·26	0·14	0·07	Yes
	2·85	57·5	46·3	4	134	0·36	6·9	0·25	0·14	0·09	Yes
	2·35	38·8	32·9	4	128	0·36	6·9	0·24	0·15	0·10	Yes
	2·45	38·4	32·4	4	107	0·36	6·9	0·24	0·14	0·07	Yes
	2·35	39·4	33·8	4	131	0·36	6·9	0·23	0·15	0·10	Yes
	2·45	43·3	38·3	4	122	0·36	6·9	0·23	0·13	0·08	Yes
	2·65	48·5	38·1	4	154	0·36	6·9	0·25	0·16	0·15	Yes
Goddard Ranch	2·2	47·3	36	4	122	0·3	6·9	0·22	0·15	0·08	Yes
	2·2	41·1	32·7	4	105	0·3	6·9	0·21	0·14	0·06	Yes

Table III. Continued

Site	Depth (m)	σ_v (kPa)	σ'_v (kPa)	Soil type	Average V_s (m/s)	Average a_{max} (g)	Mw	CSR	CRR (ANN)	CRR (Andrus)	Liquefaction observation
Andersen Bar	2	40·6	28·7	4	106	0·29	6·9	0·23	0·15	0·07	Yes
	2	39	27·8	4	105	0·29	6·9	0·23	0·15	0·07	Yes
North Gravel Bar	2·4	51	36	4	206	0·46	6·9	0·36	0·42	0·19	No
	3·65	75·2	53·5	4	274	0·46	6·9	0·35	0·42	0·29	No
Mackaay Dam, downstream toe	3·65	66·6	57·4	4	271	0·23	6·9	0·15	0·42	0·28	No
(h) *1985 Chiba-Ibaragi-Kenkyo, Japan earthquake* ($M_w = 6·0$)											
Owi Island, No. 1	6·15	105·4	59·2	2	155	0·06	6·0	0·04	0·15	0·12	No
	14·8	251·6	120·2	2	195	0·06	6·0	0·04	0·42	0·16	No
(i) 1/16/86 *Taiwan earthquake* ($M_w = 6·6$; *Event LSST* 4)											
Lotung LSST, Facility	4·5	85·4	35·4	1·5	146	0·22	6·6	0·26	0·42	0·19	No
	4·5	85·4	35·4	1·5	133	0·22	6·6	0·26	0·42	0·12	No
	4·5	85·4	35·4	1·5	127	0·22	6·6	0·26	0·42	0·10	No
	4·5	85·4	35·4	1·5	130	0·22	6·6	0·26	0·42	0·11	No
(j) 5/20/86 *Taiwan earthquake* ($M_w = 6·6$; *Event LSST* 7)											
Lotung LSST, Facility	4·5	85·4	35·4	1·5	146	0·18	6·6	0·21	0·42	0·19	No
	4·5	85·4	35·4	1·5	133	0·18	6·6	0·21	0·42	0·12	No
	4·5	85·4	35·4	1·5	127	0·18	6·6	0·21	0·42	0·10	No
	4·5	85·4	35·4	1·5	130	0·18	6·6	0·21	0·42	0·11	No
(k) 5/20/86 *Taiwan earthquake* ($M_w = 6·2$; *Event LSST* 8)											
Lotung LSST, Facility	4·5	85·4	35·4	1·5	146	0·04	6·2	0·04	0·42	0·19	No
	4·5	85·4	35·4	1·5	133	0·04	6·2	0·04	0·42	0·12	No
	4·5	85·4	35·4	1·5	127	0·04	6·2	0·04	0·42	0·10	No
	4·5	85·4	35·4	1·5	130	0·04	6·2	0·04	0·42	0·11	No
(l) 7/30/86 *Taiwan earthquake* ($M_w = 6·2$; *Event LSST* 12)											
Lotung LSST, Facility	4·5	85·4	35·4	1·5	146	0·18	6·2	0·19	0·42	0·19	No
	4·5	85·4	35·4	1·5	133	0·18	6·2	0·19	0·42	0·12	No
	4·5	85·4	35·4	1·5	127	0·18	6·2	0·19	0·42	0·10	No
	4·5	85·4	35·4	1·5	130	0·18	6·2	0·19	0·42	0·11	No
(m) 7/30/86 *Taiwan earthquake* ($M_w = 6·2$; *Event LSST* 13)											
Lotung LSST, Facility	4·5	85·4	35·4	1·5	146	0·05	6·2	0·05	0·42	0·19	No
	4·5	85·4	35·4	1·5	133	0·05	6·2	0·05	0·42	0·12	No
	4·5	85·4	35·4	1·5	127	0·05	6·2	0·05	0·42	0·10	No
	4·5	85·4	35·4	1·5	130	0·05	6·2	0·05	0·42	0·11	No

Table III. Continued

Site	Depth (m)	σ_v (kPa)	σ'_v (kPa)	Soil type	Average V_s (m/s)	Average a_{max} (g)	Mw	CSR	CRR (ANN)	CRR (Andrus)	Liquefaction observation
(n) 11/4/86 *Taiwan earthquake* ($M_w = 7{\cdot}6$; *Event LSST* 16)											
Lotung LSST, Facility	4·5	85·4	35·4	1·5	146	0·16	7·6	0·25	0·42	0·19	No
	4·5	85·4	35·4	1·5	133	0·16	7·6	0·25	0·42	0·12	No
	4·5	85·4	35·4	1·5	127	0·16	7·6	0·25	0·42	0·10	No
	4·5	85·4	35·4	1·5	130	0·16	7·6	0·25	0·42	0·11	No
(o) *1987 Chiba-Toho-Oki, Japan earthquake* ($M_w = 6{\cdot}5$)											
Sunamachi	9·1	168·2	140·2	2·5	150	0·1	6·5	0·05	0·20	0·07	No
(p) *1987 Elmore Ranch, California earthquake* ($M_w = 5{\cdot}9$)											
Wildlife	4·65	83·8	53·9	1·5	127	0·12	5·9	0·07	0·18	0·08	No
	4·65	83·8	53·9	1·5	124	0·12	5·9	0·07	0·18	0·07	No
	4·65	91·8	57·8	1·5	115	0·12	5·9	0·08	0·16	0·06	No
Radio Tower	4·4	79·2	55·8	2	90	0·11	5·9	0·06	0·13	0·04	No
McKim	3·15	54·3	38·1	2	126	0·06	5·9	0·03	0·19	0·09	No
Vail Canal	4·1	70·4	54·8	2·5	101	0·13	5·9	0·07	0·12	0·05	No
Kornbloom	4·25	74·7	57·8	1	105	0·24	5·9	0·12	0·12	0·05	No
Heber Road, channel fill	3·65	63	48	2	131	0·03	5·9	0·02	0·09	0·09	No
	3·65	63	48	2	133	0·03	5·9	0·02	0·13	0·09	No
Heber Road, point bar	3·15	60·1	46·6	2·5	164	0·03	5·9	0·02	0·20	0·19	No
	3·15	60·1	46·6	2·5	173	0·03	5·9	0·02	0·20	1·60	No
(q) *1987 Superstition Hills, California earthquake* ($M_w = 6{\cdot}5$)											
Wildlife	4·65	83·8	53·9	1·5	127	0·2	6·5	0·15	0·18	0·08	No
	4·65	83·8	53·9	1·5	124	0·2	6·5	0·15	0·18	0·07	No
	4·65	91·8	57·8	1·5	115	0·2	6·5	0·15	0·16	0·06	No
Radio Tower	4·4	79·2	55·8	2	90	0·2	6·5	0·14	0·13	0·04	No
McKim	3·15	54·3	38·1	2	126	0·19	6·5	0·13	0·19	0·09	No
Vail Canal	4·1	70·4	54·8	2·5	101	0·2	6·5	0·12	0·12	0·05	No
Kornbloom	4·25	74·7	57·8	1	105	0·21	6·5	0·13	0·12	0·05	No
Heber Road, channel fill	3·65	63	48	2	131	0·18	6·5	0·11	0·09	0·09	No
	3·65	6	48	2	133	0·18	6·5	0·11	0·13	0·09	No
Heber Road, point bar	3·15	60·1	46·6	2·5	164	0·18	6·5	0·11	0·20	0·19	No
	3·15	60·1	46·6	2·5	173	0·18	6·5	0·11	0·20	1·60	No

Table III. Continued

Site	Depth (m)	σ_v (kPa)	σ'_v (kPa)	Soil type	Average V_s (m/s)	Average a_{max} (g)	Mw	CSR	CRR (ANN)	CRR (Andrus)	Liquefaction observation
(r) *Loma Prieta, California earthquake* (M_w = 7·1)											
Treasure Island,	7·85	106·6	63·5	2	130	0·14	7·1	0·13	0·14	0·07	Marginal
fire station	8·35	148·7	83·7	2	157	0·14	7·1	0·13	0·13	0·10	Marginal
	8·35	147·2	83	2	157	0·14	7·1	0·13	0·13	0·10	Marginal
	8·35	101·3	60·9	2	131	0·14	7·1	0·12	0·14	0·08	Marginal
	8·35	118·5	69·2	2	136	0·14	7·1	0·13	0·13	0·08	Marginal
	8·35	139·9	78·6	2	148	0·14	7·1	0·13	0·12	0·09	Marginal
	8·35	163	90·6	2	137	0·14	7·1	0·13	0·12	0·07	Marginal
	8·35	154·4	86·4	2	152	0·14	7·1	0·13	0·13	0·09	Marginal
	8·35	146·3	82·5	2	146	0·14	7·1	0·13	0·12	0·08	Marginal
Treasure Island,	7·2	133·1	77·5	2·5	178	0·14	7·1	0·13	0·12	0·15	No
perimeter	5·75	102·6	71	3	163	0·15	7·1	0·12	0·15	0·11	Yes
	4	75·4	48·8	3	154	0·14	7·1	0·12	0·12	0·12	Yes
	4·55	82·1	63·9	2·5	143	0·15	7·1	0·11	0·12	0·09	Yes
Port of Richmond	6	110·1	84·7	1·5	143	0·16	7·1	0·12	0·11	0·08	Yes
	6	110·1	84·7	1·5	135	0·16	7·1	0·12	0·11	0·07	Yes
	6	97	78·8	1·5	117	0·16	7·1	0·11	0·10	0·05	Yes
	6	98·9	79·4	1·5	152	0·16	7·1	0·11	0·10	0·10	Yes
	6	98·6	79·4	2	121	0·16	7·1	0·11	0·09	0·06	Yes
	6	98·6	79·4	2	138	0·16	7·1	0·11	0·10	0·07	Yes
Port of Richmond	6	104·4	82	2	148	0·16	7·1	0·11	0·15	0·09	No
Hall Ave.	6	104·4	82	2	145	0·16	7·1	0·11	0·13	0·08	No
	6	109·2	84·3	2	133	0·16	7·1	0·12	0·11	0·07	No
Bay Bridge, Toll Plaza	6·25	115·9	82·4	2·5	134	0·24	7·1	0·19	0·13	0·07	Yes
	6·25	108·3	78·8	2·5	146	0·24	7·1	0·18	0·12	0·08	Yes
	7·5	136·6	92·4	2·5	148	0·24	7·1	0·19	0·19	0·08	Yes
Port of Oakland	6·75	121·6	85·8	3	145	0·24	7·1	0·19	0·17	0·08	Yes
	6·75	121·6	85·8	3	179	0·24	7·1	0·19	0·18	0·13	Yes
	6·75	115·8	83·1	3	157	0·24	7·1	0·18	0·16	0·09	Yes
	6·75	122·5	86·2	3	142	0·24	7·1	0·19	0·17	0·07	Yes
	6·75	122·5	86·2	3	145	0·24	7·1	0·19	0·17	0·08	Yes
	6·25	113·1	81·7	3	176	0·24	7·1	0·18	0·16	0·12	Yes
Bay Farm Island, dike	5	87·1	75·2	2·5	193	0·27	7·1	0·18	0·21	0·45	No
	5	87·1	75·2	2·5	212	0·27	7·1	0·18	0·22	0·10	No
	5	91·9	77	2·5	204	0·27	7·1	0·18	0·21	0·02	No

Table III. Continued

Site	Depth (m)	σ_v (kPa)	σ'_v (kPa)	Soil type	Average V_s (m/s)	Average a_{max} (g)	Mw	CSR	CRR (ANN)	CRR (Andrus)	Liquefaction observation
Bay Farm Island,	3·85	69·9	60·9	2·5	97	0·27	7·1	0·18	0·13	0·04	Yes
Loop Road	3·85	69·9	60·9	2·5	116	0·27	7·1	0·18	0·13	0·06	Yes
	3·85	67	59·6	2·5	125	0·27	7·1	0·17	0·15	0·07	Yes
Marina, District	3·5	61·9	54·4	3	153	0·15	7·1	0·10	0·10	0·11	Yes
	6·45	117	82·2	2·5	120	0·15	7·1	0·12	0·12	0·05	Yes
	6·45	117	82·2	2·5	105	0·15	7·1	0·12	0·11	0·04	Yes
	3·95	69·9	59·6	3	120	0·15	7·1	0·10	0·07	0·06	Yes
	7·95	140·6	105·7	3	220	0·15	7·1	0·11	0·28	0·43	No
Coyote Creek	4·75	83·6	62·1	4	136	0·19	7·1	0·15	0·07	0·08	No
	4·75	75·4	58·2	4	154	0·19	7·1	0·14	0·15	0·11	No
	4·75	75·4	58·2	4	161	0·19	7·1	0·14	0·16	0·12	No
	4·75	75·4	58·2	4	173	0·19	7·1	0·14	0·17	0·15	No
Salinas River, north	9·85	178·2	140·8	1·5	177	0·15	7·1	0·10	0·25	0·10	No
	9·85	178·2	140·8	1·5	195	0·15	7·1	0·10	0·27	0·13	No
	9·85	178·2	140·8	1·5	200	0·15	7·1	0·10	0·28	0·15	No
	9·85	178·2	140·8	1·5	199	0·15	7·1	0·10	0·27	0·15	No
Salinas River, south	8·75	142·2	123·5	2·5	131	0·15	7·1	0·09	0·21	0·05	No
	8·75	142·2	123·5	2·5	149	0·15	7·1	0·09	0·22	0·07	No
	8·75	142·2	123·5	2·5	158	0·15	7·1	0·09	0·22	0·08	No
	8·75	142·2	1230·5	2·5	168	0·15	7·1	0·09	0·22	0·09	No
Santa Cruz	2·6	48·1	28·7	2	116	0·42	7·1	0·41	0·34	0·09	Yes
	3·25	60·1	48·1	2·5	145	0·42	7·1	0·30	0·17	0·11	Yes
	2·9	51	41	2	126	0·42	7·1	0·30	0·42	0·09	No
	3·8	67·7	57·8	2	135	0·42	7·1	0·28	0·42	0·09	No
	4	69·2	49·8	2	158	0·42	7·1	0·33	0·42	0·18	No
	2·2	41	30·5	3	126	0·42	7·1	0·33	0·13	0·10	Yes

Table III. Continued

Site	Depth (m)	σ_v (kPa)	σ'_v (kPa)	Soil type	Average V_s (m/s)	Average a_{max} (g)	Mw	CSR	CRR (ANN)	CRR (Andrus)	Liquefaction observation
Mos Landing (ML),	3·2	63·6	46·9	3	116	0·25	7·1	0·20	0·09	0·07	Yes
State Beach	5·85	101·3	69·8	3	162	0·25	7·1	0·20	0·15	0·11	Yes
ML, Sandholt Rd	2·85	54·2	42·4	3	130	0·25	7·1	0·19	0·12	0·09	Yes
	7·95	148·5	87·7	3	209	0·25	7·1	0·23	0·23	0·36	No
	5·15	85·6	59·5		171	0·25	7·1	0·20	0·18	0·15	Marginal
ML, Harbor Office	3·8	74·8	53·1	2·5	150	0·25	7·1	0·20	0·15	0·11	Yes
ML, Woodward Marine	3·3	60·3	39·6	3	143	0·25	7·1	0·22	0·14	0·12	Yes
(s) *1993 Hokkaido-nansei-oki, Japan earthquake* ($M_w = 8·3$)											
Pension House	2·25	45·5	33·4	4	79	0·19	8·3	0·20	0·02	0·04	Yes
	6·1	122·9	70	4	144	0·19	8·3	0·26	0·06	0·08	Marginal
(t) *1995 Hyogo-ken Nanbu, Japan earthquake* ($M_w = 6·9$)											
Port Island,	8·7	160·8	98·8	4	197	0·5	6·9	0·41	0·25	0·19	Yes
Instrumented array	8·7	185·9	110·9	4	174	0·5	6·9	0·42	0·29	0·10	Yes
SGK (TRC)	9	158·5	139·1	3	149	0·48	6·9	0·27	0·13	0·06	No
TKS (TPS)	4·8	73·8	57·9	3	135	0·2	6·9	0·14	0·11	0·08	Yes
KNK (KPS)	10·4	193·6	111	3	179	0·12	6·9	0·10	0·24	0·11	No

Table IV. Comparison of success rates in predicting liquefaction/non-liquefaction

Percentage difference allowance†	ANN model (equaion (13))			ANN model with reduction factor of 0·8			Andrus and Stokoe[10]		
	Liquefied cases (%)	Non-liquefied cases (%)	Overall (%)	Liquefied cases (%)	Non-liquefied cases (%)	Overall (%)	Liquefied cases (%)	Non-liquefied cases (%)	Overall (%)
0	88	88	88	99	70	87	99	40	68
5	92	91	92				99	42	69
10	94	95	95				99	42	69
20	100	95	97				100	46	71

†The definition of success include cases where the method does not yield correct prediction but the difference between the calculated CRR and CSR in less than, say, 5 per cent (or 10 or 20 per cent)

seismic loads and is the basis for the development of a limit state for V_s-based liquefaction evaluation.

2. A limit state specifies the critical CSR a soil can resist without being liquefied. The proposed procedure for establishing the limit state for V_s-based liquefaction evaluation is considered satisfactory. The limit state defined by equation (13) and Table II is shown to be able to determine, accurately, the liquefaction resistance of soils reported in the Andrus and Stokoe's database. The complexity of the limit state as a function of the four variables (σ'_v, σ_v, V_s, ST), as evidenced by equation (13) and Table II, indicates that a simple empirical chart may not be established without the sacrifice of the accuracy of the liquefaction resistance prediction.
3. The ANN models developed in the present study yield more accurate predictions of liquefaction resistance than does the Andrus and Stokoe's method. Further study to quantify uncertainty of the ANN model and the V_s-based limit state for liquefaction, particularly on the use of attenuation model in the development of limit state, and to investigate its effect by performing probabilistic analyses is warranted so that a rational design guideline may be established.

ACKNOWLEDGMENTS

The study on which this paper is based is supported by the National Science Foundation through Grant No. CMS-9612116. The cognizant NSF program official for this grant is Dr. Clifford Astill. This financial support is greatly appreciated. The authors are in debt to Dr. Ronald D. Andrus for his kindness in providing fines contents data to supplement his database.

APPENDIX—SAMPLE CALCULATION IN APPLYING THE DEVELOPED NEURAL NETWORK

Using data at Salinas Rover, North site in 1906 San Francisco, California, Earthquake (see Table III) as an example, CRR is calculated as follows:

$$\text{Given: } \sigma_v = 178{\cdot}2\ \text{kPa},\ \sigma'_v = 140{\cdot}8\ \text{kPa},\ V_s = 177\ \text{m/s, and SCN} = 1{\cdot}5.$$

Step 1: Input variables.

$$P_1 = \sigma_v/\sigma'_v = 1{\cdot}266,\ P_2 = \sigma'_v = 140{\cdot}8,\ P_3 = \text{SCN} = 1{\cdot}5, \text{ and } P_4 = V_s/\sigma'_v = 1{\cdot}257.$$

Step 2: Normalization of input variables.

For the variable P_1, the coefficients a and b in equation (4) are $-0{\cdot}955$ and 1.61, thus

$$P_{1N} = (P_1 - 0{\cdot}955)/1{\cdot}61 = 0{\cdot}193$$

For the variable P_2, the coefficients a and b in equation (4) are $-13{\cdot}675$ and 141·25, thus

$$P_{2N} = (P_2 - 13{\cdot}675)/141{\cdot}25 = 0{\cdot}900$$

For the variable P_3, the coefficients a and b in equation (4) are $-0{\cdot}625$ and 3·75, thus

$$P_{3N} = (P_3 - 0{\cdot}625)/3{\cdot}75 = 0{\cdot}233$$

For the variable P_4, the coefficients a and b in equation (4) are $-0{\cdot}4775$ and 5·825, thus

$$P_{4N} = (P_4 - 0{\cdot}4775)/5{\cdot}825 = 0{\cdot}134$$

Note that these coefficients (a and b) are derived based on the entire database.

Step 3: Calculation of CRR by using equation (13) and normalized P_i values

$\mathrm{CRR}_N = 0{\cdot}5799$ (obtained by a simple spreadsheet; the spreadsheet template available upon request)

Step 4: Denormalization of CRR.

$$\mathrm{CRR} = (\mathrm{CRR}_N - 0{\cdot}022)/0{\cdot}398 = 0{\cdot}253$$

REFERENCES

1. H. B. Seed and I. M Idriss, 'Simplified procedure for evaluating soil liquefaction potential', *J. Soil Mech. Found. Div. ASCE* **97**(SM 9)**,** 1249–1273 (1971).
2. H. B. Seed and I. M. Idriss, *Ground Motions and Soil Liquefaction During Earthquake*, Monograph Series, Earthquake Engineering Research Institute, Berkeley, California, 1982.
3. R. O. Davis and J. B. Berrill, 'Comparison of a liquefaction theory with field observations', *Geotechnique*, **33,** 455–460 (1983).
4. R. O. Davis and J. B. Berrill, 'Energy dissipation and seismic liquefaction in sands', *Earthquake Engng. Struct. Dyn.*, **10,** 59–68 (1982).
5. C. S. Desai and Y. Ma, 'Modeling of joints and interfaces using the disturbed state concept', *Int. J. Numer. Anal. Mech. Geomech.*, **16** (7)**,** 623–653 (1992).
6. C. S. Desai, 'Constitutive modelling using the disturbed state as microstructure self-adjustment concept', in H. B. Muhlhaus (ed.), *Continum Models for Materials with Microstructure*, Chapter 8, Wiley, France, 1995.
7. D. R. Katti and C. S. Desai, 'Modeling and testing of cohesive soil using the disturbed state concept', *J. Eng. Mech. ASCE*, **121**(5)**,** 648–658 (1995).
8. C. S. Desai and J. Toth, 'Disturbed state constitutive modeling based on stress-strain and nondestructive behavior', *Int. J. Solids Struct.*, **33**(11)**,** 1619–1650 (1996).
9. C. S. Desai, I. Park and C. Shao, 'Fundamental yet simplified model for liquefaction instability', *Int. J. Numer. Anal. Mech. Geomech.*, **22,** 721–748 (1998).
10. R. D. Andrus and K. H. Stokoe, 'Liquefaction resistance based on shear wave velocity', in T. Leslie Youd and Izzat M. Idriss (eds), *Proc. NCEER Workshop on Evaluation of Liquefaction Resistance of Soils, Technical Report NCEER-97-0022*, National Center for Earthquake Engineering Research, State University of New York at Buffalo, Buffalo, NY, 1997, pp. 89–128.
11. K. H. Stokoe, J. M. Roesset, J. G. Bierschwale and M. Aouad, 'Liquefaction potential of sands from shear wave velocity', *Proc. 9th World Conf. Earthquake Eng. Vol.* III, Tokyo, Japan, 1988, pp. 213–218.
12. K. Tokimatsu, S. Kuwayama and S. Tamura, 'Liquefaction potential evaluation based on Rayleigh wave investigation and its comparison with field behavior', in S. Prakash (ed.), *Proc. 2nd Int. Conf. on Recent Advances in Geotechnical Earthquake Engineering and Soil Dynamics, St. Louis*, University of Missouri at Rolla, Missouri, *Vol.* I, 1991, pp. 357–364.
13. P. K. Robertson, D. J. Woeller and W. D. L. Finn, 'Seismic cone penetration test for evaluating liquefaction potential under cyclic loading', *Can. Geotech. J.*, **29,** 686–695 (1992).
14. R. E. Kayen, J. K. Mitchell, R. B. Seed, A. Lodge, S. Nishio and R. Coutinho, 'Evaluation of SPT-, CPT-, and shear wave-based methods for liquefaction potential assessment using Loma Prieta data', in M. Hamada and T. D. O'Rourke (eds), *Proc. 4th Japan – U.S. Workshop on Earthquake Resistance Design of Lifeline facilities and Countermeasures for soil liquefaction, Technical Report NCEER-92-0019*, National Center for Earthquake Engineering Research, State University of New York, Buffalo, New York 1992, pp. 177–204.
15. R. D. Andrus, 'In situ characterization of gravelly soils that liquefied in the 1983 Borah Peak Earthquake', *Ph.D. Dissertation*, University of Texas, Austin, 1994.
16. A. L. Lodge, 'Shear wave velocity measurements for subsurface characterization', *Ph.D. Dissertation*, University of California, Berkeley, CA, 1994.
17. P. K. Robertson and C. E. Wride, 'Cyclic liquefaction and its evaluation based on the SPT and CPT', in T. Leslie Youd and Izzat M. Idriss (eds.), *Proc. NCEER Workshop on Evaluation of Liquefaction Resistance of Soils, Technical Report NCEER-97-0022*, National Center for Earthquake Engineering Research, State University of New York at Buffalo, Buffalo, New York, 1997, pp. 41–87.
18. R. S. Olsen, 'Cyclic liquefaction based on the cone penetrometer test', in T. Leslie Youd and Izzat M. Idriss (eds.), *Proc. NCEER Workshop on Evaluation of Liquefaction Resistance of Soils, Technical Report NCEER-97-0022*, National Center for Earthquake Engineering Research, State University of New York at Buffalo, Buffalo, New York, 1997, pp. 225–276.

19. S. S. C. Liao, D. Veneziano and R. V. Whitman, 'Regression models for evaluating liquefaction probability', *ASCE J. Geotech. Engng*., **114**(4), 389–411 (1988).
20. T. L. Youd and S. K. Noble, 'Liquefaction criteria based on statistical and probabilistic analyses', in T. Leslie Youd and Izzat M. Idriss (eds.), *Proc. NCEER Workshop on Evaluation of Liquefaction Resistance of Soils*, *Technical Report NCEER-97-0022*, National Center for Earthquake Engineering Research, State University of New York at Buffalo, Buffalo, New York, 1997, pp. 201–215.
21. C. H. Juang, D. V. Rosowsky and W. H. Tang, 'A reliability-based method for assessing liquefaction potential of sandy soil', ASCE *J. Geotech. Geoenviron. Eng.* **125**(8), 684–689 (1999).
22. R. S. Olsen, 'Normalization and prediction of geotechnical properties using the cone penetrometer test', *Final Report*, U.S. Army Corps of Engineers, Waterways Experiment Station, Vicksburg, MS, 1994.
23. A. T. C. Goh, 'Seismic liquefaction potential assessed by neural networks', *J. Geotech. Engng. ASCE*, **120**(9), 1467–1480 (1994).
24. A. T. C. Goh, 'Neural network modeling of CPT seismic liquefaction data', *J. Geotech. Engng. ASCE* **122**(1), 70–73 (1996).
25. C. H. Juang and C. J. Chen, 'CPT-based liquefaction evaluation using artificial neural networks', *J. Comput. Aided Civ. Infras. Eng*., **14,** 221–229 (1999).
26. C. H. Juang, C. J. Chen and Y. M. Tien, 'Appraising CPT-based liquefaction resistance evaluation methods—artificial neural network approach', *Can. Geotech. J*., **36**(3), (1999).
27. Y. M. Najjar and E. A. Hossam, 'CPT-based liquefaction potential assessment: a neuronet approach', ASCE Geotechnical Special Publication No. 75, Geotechnical Earthquake Engineering and Soil Dynamics III, 1998, pp. 542–553.
28. H. Demuth and M. Beale, Neural Network Toolbox User's Guide, The Math Works, Natick, MA, 1996.
29. MATLAB User's Guide. The Math Works, Natick, MA, 1998.
30. I. M. Idriss, 'Evaluation of liquefaction potential, consequences and mitigation—an update', Presentation Notes, Vancouver Geotechnical Society Meeting, Vancouver, B.C., February 17, 1998.
31. K. W. Campbell, 'Near-surface attenuation of peak horizontal acceleration', *Bull. Seismol. Soc. Am*., **71**(6), 2039–2070 (1981).

